JOURNAL OF COMPUTATIONAL PHYSICS 59, 120–135 (1985)

Recursive Residue Generation Method for Laser–Molecule Interaction: Utilization of Structured Sparsity*

JOSÉ E. CASTILLO

Departments of Computer Science and Mathematics, University of Texas, Austin, Texas 78712

AND

ROBERT E. WYATT

Department of Chemistry and Institute for Theoretical Chemistry, University of Texas, Austin, Texas 78712

Received February 7, 1984; revised May 24, 1984

The recursive residue generation method (RRGM) permits the generation of time-dependent transition amplitudes in many-state quantum systems. An important step in the method utilizes the Lanczos algorithm to tridiagonalize the matrix representation of the Hamiltonian. Analysis of this sparse matrix, for a generic laser–molecule Hamiltonian, revealed structure (repeating blocks of elements in each off-diagonal) which allowed for greatly reduced storage. In addition, utilization of this structure for construction of a smart matrix–vector multiplier then permitted calculations on systems with very large bases ($\sim$40,000). Time-dependent transition probabilities are shown for excitation into several bands of states in a system with over 3000 states.

1. INTRODUCTION

The recursive residue generation method (RRGM) is a recently formulated approach to the computation of time-dependent transition amplitudes in many-state quantum systems [1, 2]. In many-state quantum dynamics (a diverse subject which includes molecular multiphoton excitation, the influence of relaxation processes on spectral line shapes, and the interaction of adsorbed particles with surface vibration-electronic states), the principal limitation has been the inability to routinely obtain eigenvectors of large symmetric ($>$1000 rows or columns) matrices. In the RRGM, transition amplitudes are computed one at a time by recursively generating the residues of several Green functions; eigenvectors of large

* Supported in part by the Robert A. Welch Foundation of Houston, Tex., and the National Science Foundation.

0021-9991/85 $3.00

matrices are not computed at all. An important step in the RRGM is tridiagonalization of the Hamiltonian matrix, for which the Lanczos algorithm [3–8] is admirably suited.

In our previous studies [1, 2], we either stored all nonzero elements of the sparse Hamiltonian matrix in fast storage, or we repeatedly read batches (10–20,000 at a time) of matrix elements from disk into fast storage. In the former case, systems with up to about 12,000 states could be readily handled (on the CYBER 170/750), but we would like to be able to deal with systems involving many more ($>50{,}000$) states. To overcome this limitation on our earlier calculations, we closely examined the structure of the sparse matrices associated with a generic molecular Hamiltonian. The *structured sparsity* discovered as a result of this analysis appeared as repeating sets of nonzero elements in each of the off-diagonals of the Hamiltonian matrix. In addition to allowing for very compact storage of the Hamiltonian matrix, this structure permits the design and implementation of a smart matrix–vector multiplier which in turn greatly accelerates the most time consuming (Lanczos resursion) aspect of the RRGM. As a result, it is now possible to extend dynamical studies to systems with $\sim 40{,}000$ states. Although this type of structure in the Hamiltonian matrix depends upon the problem (i.e., Hamiltonian operator) under consideration, the concept of utilizing structure in the off-diagonal elements transcends our specific application.

The Lanczos algorithm plays a central role in the RRGM. Over the past decade, a greater appreciation of its powers has arisen through applications to such diverse topics as: electronic and phonon state densities in solid state physics [9–11], the dynamic Jahn–Teller effect [12, 17], molecular vibrational energies [18], magnetic relaxation lineshapes [19–22], electronic excitation–ionization spectra [23], and the calculation of optical potentials [24].

In Section II, the RRGM for laser–molecule interaction is presented in more detail than in an earlier study [1]. Structure in the sparse Hamiltonian matrix is described in Section IIB. Section IIC reviews the RRGM, while Section IID concentrates on utilizing the Lanczos method for large scale computations. Then, in Section III, for the Hamiltonian described in Section IIA, numerical results are presented for probabilities of excitation into bands of excited states. A brief summary appears in Section IV.

II. Theory

A. *Model Hamiltonian*

A reasonable model for the interaction of a monochromatic laser with a multimode molecule involves a classical electromagnetic field, dipole coupled to an anharmonic pump mode, which in turn is linearly coupled to a multimode harmonic bath. The total Hamiltonian is the sum of a molecular (time-independent) term and a time-dependent driving term,

$$H(t) = H_m + H'(t), \tag{1}$$

where

$$H_m = \hbar\omega_a[(a^\dagger a) - x(a^\dagger a)^2] + \sum_{i=1}^{n_\beta} \hbar\omega_i b_i^\dagger b_i + \sum_{i=1}^{n_\beta} V_i(a^\dagger b_i + a b_i^\dagger) \tag{2}$$

and, for $t \geqslant 0$,

$$H'(t) = V_{\text{rad}}(a + a^\dagger)\cos\omega_l t. \tag{3}$$

In these equations, $\{a^\dagger, a\}$ and $\{b_i^\dagger, b_i\}$ are raising and lowering operators for the pump mode and the ith bath mode, respectively. The anharmonic mode has a (zero-order) frequency ω_a and anharmonicity parameter x. The third term in Eq. (2) is the Hamiltonian for n_β uncoupled bath modes, while the fourth term provides intramolecular vibrational coupling between the pump mode and each bath mode. Finally, in Eq. (3), $V_{\text{rad}} = \mu_0 E_0$ determines the strength of the linear dipole coupling $(a + a^\dagger)$ between the laser, of frequency ω_l and field strength E_0, and the pump mode. This Hamiltonian and its variants have been used before in studies of laser-molecule and laser-adatom interaction [25, 26].

If $|n\rangle$ denotes a harmonic basis state, where $n = 0, 1, 2,...$, then the well-known matrix elements (analogous expressions involve $b_i^\dagger$ and b_i) [27] over $a^\dagger$ and a allow simple evaluation of all matrix elements involving operators for a single mode. For the mulitmode problem, products of harmonic basis states

$$|n_a\rangle\,|n_1\rangle \cdots |n_\beta\rangle,$$

where $|n_a\rangle$ denotes a pump mode state, and $|n_i\rangle$ is an n_i phonon state for the ith bath mode, form a basis for representing the complete Hamiltonian. In the matrix representation of H_m, the first three terms, denoted $H_a + H_b$ (anharmonic + bath), in Eq. (2) will produce only diagonal elements, while the last term, denoted H_c (coupling), produces only off-diagonal elements.

It is very convenient to attach a single index to the vector of quantum numbers $\{n_a, n_1,..., n_\beta\}$ representing one basis element. If D_p represents the maximum number of states allowed in the pth bath mode, then the single integer m attached to a basis element is [28]

$$m = (n_a + 1) + D_1 n_1 + D_1 D_2 n_2 + \cdots + D_1 D_2 \cdots D_\beta n_\beta. \tag{4}$$

For example, in a system with one pump mode and two bath modes in which only the ground and first excited state are allowed in the basis ($D_1 = D_2 = 2$),

$$m = (n_a + 1) + 2n_1 + 4n_2,$$

so that the 8 basis elements, as m ranges from 1 to 8 are: $|0\rangle\,|0\rangle\,|0\rangle$, $|1\rangle\,|0\rangle\,|0\rangle$, $|0\rangle\,|1\rangle\,|0\rangle$, $|1\rangle\,|1\rangle\,|0\rangle$, $|0\rangle\,|0\rangle\,|1\rangle$, $|1\rangle\,|0\rangle\,|1\rangle$, $|0\rangle\,|1\rangle\,|1\rangle$, and $|1\rangle\,|1\rangle\,|1\rangle$. Of course, the indexing scheme attached to the basis elements determines the pat-

tern of nonzero elements in the matrix representation of the Hamiltonian. We will return to this point in Section IIC.

The transition amplitude $A_{fi}(t)$ between basis state $|i\rangle$ at $t=0$ and basis state $|f\rangle$ at time t is a matrix element of the propagator $U(t|0)$ [29],

$$A_{fi}(t) = \langle f|U(t|0)|i\rangle. \tag{5}$$

The propagator solves the Schrödinger equation subject to the initial condition $U(0|0)=1$. For times which are multiples of the laser period $\tau = 2\pi/\omega_l$, the ρ-cycle propagator is obtained through products of one-cycle propagators,

$$U(\rho\tau|0) = [U(\tau|0)]^{\rho}. \tag{6}$$

This means that if the propagator over one cycle can be found, then propagation to the end of ρ cycles follows directly from Eq. (6). An exponential solution for the propagator, which facilitates utilization of Eq (6), is provided by the Magnus series [31, 32],

$$U(\tau|0) = \exp[-i\Omega(\tau)/\hbar] = \exp[-i(\Omega_1(\tau) + \Omega_2(\tau) + \cdots)/\hbar)], \tag{7}$$

where the first and the second order terms are,

$$\begin{aligned} \Omega_1(\tau) &= \int_0^{\tau} H(t_1)\, dt_1, \\ \Omega_2(\tau) &= \frac{i}{2\hbar}\int_0^{\tau} dt_2 \int_0^{t_2} [H(t_1), H(t_2)]\, dt_1. \end{aligned} \tag{8}$$

It is convenient to define the quasi-energy operator [34, 35] as the effective *time-independent* Hamiltonian which advances the system through one laser cycle:

$$U(\tau|0) = \exp[-iM\tau/\hbar]. \tag{9}$$

Comparing Eqs. (7) and (9), $M = \Omega(\tau)/\tau$. It can be shown that M is a real, Hermitian operator [2]. In addition, ρ-cycle propagation now follows trivially from Eq. (6)

$$U(\rho\tau|0) = \exp[-iM\rho\tau/\hbar]. \tag{10}$$

Using the Hamiltonian in Eqs. (1)–(3), the quasi-energy operator, through the third order, is [2]

$$M = H_m - \frac{1}{\hbar^2\omega^2}\{[H_m, [H_m, H_r]] - \tfrac{1}{4}[H_r, [H_m, H_r]]\} \tag{11}$$

or, in terms of matrix elements within the zero-order molecular basis,

$$M_{pq} = E_p^0\,\delta_{pq} + (H_c)_{pq} - (H_r)_{pq} - (H_r)_{pq}[(E_p^0 - E_q^0)/\hbar\omega_l]^2, \tag{12}$$

TABLE I

PARAMETERS IN HAMILTONIAN[a]

$\hbar\omega_a$	Pump mode fundamental	1.00
x	Pump mode anharmonicity	0.01
$\hbar\omega_i$	Bath mode frequencies	0.97, 0.99, 1.01, 1.03
V_i	Intramolecular coupling[b]	0.03, 0.06, 0.12, 0.15
V_{rad}	Radiative coupling	0.12

[a] See Eqs. (2), (3).

[b] The intramolecular coupling was the same for all four bath modes, but assumed the values listed here.

which is correct through the lowest orders in the intramolecular and radiative coupling operators,

$$H_c = \sum_{i=1}^{n_\beta} V_i(a^\dagger b_i + a b_i^\dagger),$$
$$H_r = V_{\text{rad}}(a + a^\dagger) \tag{13}$$

The structure of the effective Hamiltonian matrix defined in Eq. (12) will be analyzed in the next section. Recently, we have avoided the Magnus approximation by working with a quantized radiation field, instead of the classical field in Eq. (3). However, the off-diagonal elements have the same structure as the operator in Eq. (12).

Parameters in this Hamiltonian are listed in Table I. In addition, we will only consider $n_\beta = 4$, i.e., four bath modes coupled to the pump mode. For bath frequencies near the pump mode fundamental, the states cluster into quasidegenerate bands near $E = 0, 1, 2,...$, with 1 state in the lowest band (Band 1), 5 states in Band 2, 15 states in Band 3, etc.

B. *RRGM: Review* [1, 2]

In this section, we will present a brief review of the RRGM [1, 2]. An outline of the steps is shown in Fig. 1. From Eq. (5), the quantum mechanical transition amplitude between initial state $|i\rangle$ at time $t = 0$ and final state $|f\rangle$ at time t is given by

$$\langle f | e^{-iMt/\hbar} | i \rangle = \sum_\alpha \langle f | \alpha \rangle \langle \alpha | i \rangle \, e^{-iE_\alpha t/\hbar}, \tag{14}$$

where $\{|\alpha\rangle, \alpha = 1, 2,..., N\}$ denotes the set of eigenstates of M, $M|\alpha\rangle = E_\alpha |\alpha\rangle$. In the RRGM, direct calculation of the eigenvector coefficients $\langle f | \alpha \rangle$ is avoided. Instead, we focus upon the *transition residues* (a real Hamiltonian and real-valued basis elements are assumed).

$$R_{fi}(\alpha) = \langle f | \alpha \rangle \langle \alpha | i \rangle = \tfrac{1}{2}[\langle u_0 | \alpha \rangle^2 - \langle v_0 | \alpha \rangle^2] = \tfrac{1}{2}[R_u(\alpha) - R_v(\alpha)], \tag{15}$$

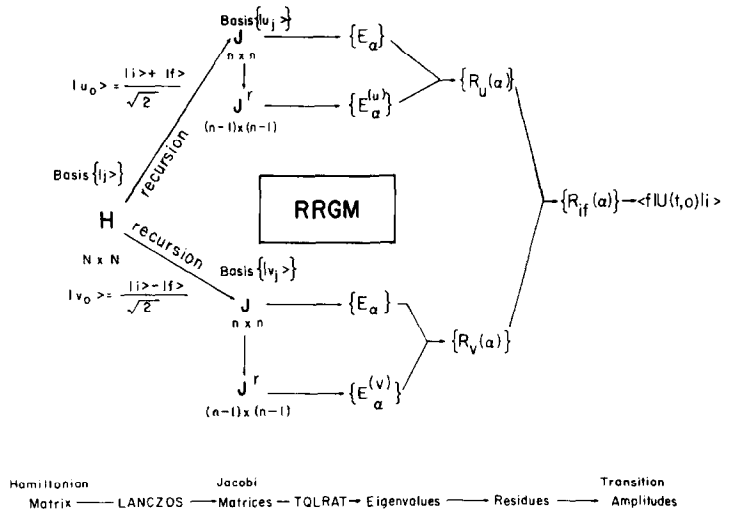

FIG. 1. RRGM flowchart.

where the two *transition vectors* are

$$|u_0\rangle = [|i\rangle + |f\rangle]/\sqrt{2},$$
$$|v_0\rangle \doteq [|i\rangle - |f\rangle]/\sqrt{2}, \tag{16}$$

The quantities $R_u(\alpha)$, $R_v(\alpha)$, and $R_{fi}(\alpha)$ are residues, at pole E_α, of the diagonal or off-diagonal matrix elements of the Green operator $(z-M)^{-1}$, where z does not belong to the spectrum of M; for example,

$$G_u(z) = \langle u_0 | (z-M)^{-1} | u_0 \rangle = \sum_\alpha \frac{\langle u_0 | \alpha \rangle^2}{z - E_\alpha},$$
$$G_{fi}(z) = \langle f | (z-M)^{-1} | i \rangle = \sum_\alpha \frac{\langle f | \alpha \rangle \langle \alpha | i \rangle}{z - E_\alpha}, \tag{17}$$

If the Green function $G_u(z)$ is known, it is a trivial matter to extract the set of residues

$$R_u(\alpha) = \lim_{z \to E_\alpha} (z - E_\alpha)\, G_u(z) = \lim_{z \to E_\alpha} (z - E_\alpha) \langle u_0 | (z-M)^{-1} | u_0 \rangle. \tag{18}$$

The problem is to first calculate $G_u(z)$ and $G_v(z)$; residues $\{R_v(\alpha)\}$ and $\{R_v(\alpha)\}$ can then be extracted from Eq. (18), and the time-dependent transition amplitudes can be computed from Eqs. (15) and (14).

To produce $G_u(z)$, image the construction of a new orthonormal basis (the *recur-*

sion basis), $\{|u_j\rangle; j = I,..., N\}$, from the original "molecular" basis. In this new basis, the equation defining the $N \times N$ Green matrix is,

$$(z\mathbf{1} - \boldsymbol{M})\,\mathbf{G}(z) = 1, \tag{19}$$

where **G** has elements which are the Green functions, $G_{ij}(z) = \langle u_i | (z - M)^{-1} | u_j \rangle$. Each matrix in this equation can be very large, so direct computation of **G** is not feasible. However, the key point is that we need *only* the 1,1 element in the **G** matrix; this is the element previously denoted $G_u(z)$. Now, by the usual procedure to invert matrices,

$$G_u(z) = \det[z\mathbf{1} - \mathbf{M}]^r / \det[z\mathbf{1} - \mathbf{M}], \tag{20}$$

where superscript r denotes the reduced matrix obtained by deleting the first row and column from $(z\mathbf{1} - \mathbf{M})$. In terms of eigenvalues of **M** and $\mathbf{M}^r$, denoted $\{E_\alpha\}$ and $\{E_\alpha^{(u)}\}$, respectively, the ratio of determinants becomes

$$G_u(z) = \frac{(z - E_1^{(u)}) \cdots (z - E_{N-1}^{(u)})}{(z - E_1) \cdots (z - E_N)}. \tag{21}$$

Note that there are $(N-1)$ products in the numerator, and N products in the demoninator. This result, when combined with Eq. (18), permits the evaluation of residues in terms of *eigenvalues* (not eigenvectors),

$$R_u(\alpha) = \frac{(E_\alpha - E_1^{(u)})}{(E_\alpha - E_1)} \cdots \frac{(E_\alpha - E_{\alpha-1}^{(u)})(E_\alpha - E_\alpha^{(u)})}{(E_\alpha - E_{\alpha-1})(E_\alpha - E_{\alpha+1})} \cdots \frac{(E_\alpha - E_{N-1}^{(u)})}{(E_\alpha - E_N)}. \tag{22}$$

The significant result is that all residues associated with $G_u(z)$ may be computed from two sets of eigenvalues, $\{E_\alpha\}$ and $\{E_\alpha^{(u)}\}$; no eigenvectors are needed. In a similar way, residues associated with $G_v(z)$ may be computed from $\{E_\alpha\}$ and $\{E_\alpha^{(v)}\}$.

The only remaining feature to be discussed (Section IID) is how to construct the two recursion bases, $\{|u_j\rangle\}$ and $\{|v_j\rangle\}$. For this, we use the powerful Lanczos method [3, 4], which builds the new vectors, one at a time, from the old ones in such a way that the Hamiltonian matrix is converted to tridiagonal (Jacobi) form. Initiated with the starter $|u_0\rangle$, n-step Lanczos recursion simultaneously builds elements in the $n \times n$ Jacobi matrix **J** and the recursion vectors $\{|u_0\rangle, |u_1\rangle,..., |u_{n-1}\rangle\}$, which span the n-dimensional subspace V_n. Obtaining eigenvalues $\{E_\alpha\}$ from **J** and $\{E_\alpha^{(u)}\}$ from $\mathbf{J}^r$ is computationally not demanding, as discussed in the next section.

Moro and Freed, in connection with their use of the Lanczos algorithm to generate ESR spectra [21, 22], mentioned that the Lanczos method can be viewed in two ways: (1) as a *numerical algorithm* to tridiagonalize symmetric matrices, (2) "a *theoretical method* that can concisely extract the relevant information from a general description of physical systems." With regard to the latter view, they introduced the concept of the *optimal reduced space* (ORS). This is the subspace

with the *least* dimension (n), for a specified $N \times N$ matrix **M**, that generates results (in our case, transition probabilities) correct to within a fixed accuracy of the full problem. As n increases, the Lanczos algorithm constructs subspaces V_n that progressively approximate the ORS.

C. *Structured Sparsity*

Analysis of the quasi-energy matrix described in the previous section showed a sparse, real-valued, symmetric matrix with nonzero values along the diagonal and five off-diagonals in the upper triangle. If we allow a maximum of N_a states in the pump mode and a maximum of N_b in each bath mode, then the total basis size is $N = N_a(N_b)^{n_\beta}$. For the computations in Section III, $n_\beta = 4$, so that $N = N_a(N_b)^4$. The sparsity of M is illustrated in the following example: if $N_a = N_b = 5$, then $N = 3125$ but there are only 24,125 nonzero matrix elements (0.25%) out of a total of 9,765,625. In the first version of our code, all of the nonzero elements of **M** were stored as a vector [1]. In addition, a vector of integers, ICOL, gave the column index of each nonzero matrix element. However, unlike many sparse matrix storage algorithms [25], it was not necessary to store the number of nonzero elements in each row; the reason is that whenever ICOL *decreased*, the next matrix element *must* lie in the next row.

A much more efficient way to store and utilize **M** was apparent after analyzing the structure of each of the five off-diagonals. If we let the integer N_d denote the *displacement* of the dth off-diagonal to the right side of the diagonal, then we will be in a position to describe the location and structure of each off-diagonal.

First off-diagonal ($N_1 = 1$). There is a vector of elements, denoted A, of lenth N_a, which is repeated $(N-1)/N_a$ times as we advance down this off-diagonal. This off-diagonal arises *only from radiative coupling* and vector A is (for $N_a = 5$, $N_b = 3$)

$$A = V_{\text{rad}} \cdot (\sqrt{1}, \sqrt{2}, \sqrt{3}, \sqrt{4}, 0). \tag{23}$$

Second off-diagonal ($N_2 = N_a$). This off-diagonal, and the three higher ones, arise *only from intramolecular coupling between the pump mode and one of the bath modes.* The second off-diagonal arises from pump-bath mode 1 coupling, $V_1(a^\dagger b_1 + a b_1^\dagger)$. This off-diagonal has N_b vectors, which for the case $N_b = 3$ are denoted B_1, C_1, and D_1, each of length N_a, with the whole unit, of length $N_b \cdot N_a$, repeated $(N_b^4 - 1)/N_b$ times as we advance down the off-diagonal. For $N_a = 5$, $N_b = 3$, these vectors are

$$\begin{aligned} B_1 &= V_1 \cdot \{0, \sqrt{1}, \sqrt{2}, \sqrt{3}, \sqrt{4}\}, \\ C_1 &= V_1 \cdot \{0, \sqrt{2}, \sqrt{4}, \sqrt{6}, \sqrt{8}\}, \\ D_1 &= V_1 \cdot \{0, 0, 0, 0, 0\}. \end{aligned} \tag{24}$$

Note that the last vector is zero-valued.

Third off-diagonal ($N_3 = N_a N_b$). This off-diagonal arises from pump mode-bath mode 2 interaction. With V_2 replacing V_1 in the above equations, we obtain vectors B_2, C_2, and D_2. The third off-diagonal then consists of the set: vector B_2 repeated

N_b times, followed by vector C_2 repeated N_b times, followed by vector D_2 again repeated N_b times. This whole unit, of length $N_a N_b^2$, is then repeated $(N_b^3 - 1)/N_b$ times to *fill the off-diagonal.*

Fourth off-diagonal ($N_4 = N_a N_b^2$). This off-diagonal consists of vector $B_3 (= V_3 \cdot B_2/V_2)$ repeated N_b^2 times, followed by vector C_3 repeated N_b^2 times, followed by vector D_3 repeated N_b^2 times; *this* whole unit, of length $N_a N_b^3$, is then repeated $(N_b^2 - 1)/N_b$ times to fill the off-diagonal.

Fifth off-diagonal ($N_5 = N_a N_b^3$). This off-diagonal consists of vector B_4 repeated N_b^3 times, vector C_4 repeated N_b^3 times, followed by vector D_4 repeated N_b^3 times. This whole unit, of length $N_a N_b^4$, is *not* repeated.

In the previous work [1], we read all nonzero matrix elements from a disk file. However, in this study, all computations are done with fast memory, without the use of secondary storage, so direct comparisons of computer times are not meaningful. By using the repeated block structure in each off-diagonal, we were able to cut the storage from $O(N^2)$ if all elements are stored, to $\sim 6N$ if the diagonal and 5 off-diagonals are stored, to finally: the main diagonal (N), plus one vector of length N_a for the first off-diagonal, plus one vector of length $N_a(N_b - 1)$ for the 4 bath mode off-diagonals (we do not store the zero block D_1 in the bath off-diagonals). The total storage is only $N + N_a + N_a(N_b - 1)$, a number clearly much smaller than either $O(N^2)$ or $6N$. Compact storage schemes, and the use of a good matrix multiplier are keys to efficiently executing large eigen-system calculations in this and other [3] problems. Although the above description of structured sparsity is particular to the generic Hamiltonian in Eqs. (2), (3), other more complicated algebraic Hamiltonians, which are sums of products of raising and lowering operators, $(b_i^\dagger)^m (b_j)^n$, when represented in product bases $|n_1\rangle |n_2\rangle \cdots |n_N\rangle$, will also have off-diagonals with repeated symmetry blocks. For the efficiency of both storage and matrix multiplication, we highly recommend that one take advantage of this structure.

D. *Computational Techniques*

Standard techniques for solving eigenstate problems (e.g., those in the EISPACK library) are only useful for relatively small problems ($N < 250$, where N is the order of the matrix $\mathbf{M}$), mainly because storage increases as $O(N^2)$, while the number of operations increases as $O(N^3)$. The Lanczos recursion method is a viable approach to large ($N \gg 250$) problems of this type. When implementing the Lanczos method, it is important to take advantage of the sparsity of $\mathbf{M}$ by means of an efficient matrix-vector multiplier. Our utilization of Lanczos recursion is based upon the version which requires only 2 n-vectors [4, 6]; in addition, we developed a sophisticated multiplier which takes advantage of the previously described sparsity pattern. Another important aspect of this study is that we can easily change the number of bath modes and still carry on with the whole process of obtaining eigenvalues and residues, *without increasing the storage requirements.* Results obtained with increasing values of n_β will be presented elsewhere [37].

To generate the sets of eigenvalues needed to compute residues in Eq. (20), we will use the Lanczos recursion method [4, 6] to convert the Hamiltonian matrix **M** into a Jacobi (tridiagonal) matrix, **J**. Once the diagonal $\{a_0, a_1,...\}$ and off-diagonal $\{b_1, b_2,...\}$ elements of **J** have been computed, the eigenvalues are obtained quickly (in about 10% of the total CPU time) and with no additional storage by use of the EISPACK routine TQLRAT. Tridiagonalizing **M** is best viewed as arising from a transformation from the original molecular basis $\{|k\rangle, k=1, 2,..., N\}$ to the *recursion basis* $\{|n\rangle, n=0, 1,..., N-1\}$. In this new basis, the only nonzero matrix elements of **M** are the diagonal *self-energies* (a_n) and the nearest-neighbor *coupling energies* (b_n). In effect, we have converted the original problem, with a complex network of interstate couplings, to a *one-dimensional disordered lattice.* We will refer to a_n and b_{n+1} as specifying *one link in this* 1D *chain used to portray* **J** (e.g., see [10]).

In the Lanczos algorithm, each recursion step "*forges a new link in the chain.*" Starting with the initial recursion vector $|0\rangle$, after forming the vector $\mathbf{M}|0\rangle$, the first self energy is $a_0 = \langle 0|\,\mathbf{M}\,|0\rangle$. The residual vector $\{\mathbf{M}|0\rangle - |0\rangle a_0\}$ is then formed; its norm determines the first coupling element in J, $b_1 = \|\mathbf{M}|0\rangle - |0\rangle a_0\|^{1/2}$. The next normalized recursion vector is then $|1\rangle = (\mathbf{M}|0\rangle - |0\rangle a_0)/b_1$. Now, given the recursion vectors $|n\rangle$ and $|n-1\rangle$, and the previous chain link (a_{n-1}, b_n) in fast storage, the next chain link is then generated from the explicit three-term recurrence relation

$$|n+1\rangle = \{\mathbf{M}|n\rangle - |n\rangle a_n - |n-1\rangle b_n\}/b_{n+1}, \tag{25}$$

where $a_n = \langle n|\,\mathbf{M}\,|n\rangle$, and b_{n+1} normalizes the *residual vector*, $\{\mathbf{M}|n\rangle - |n\rangle a_n - |n-1\rangle b_n\}$. By construction, at least in infinite precision arithmetic, each recursion vector is implicitly orthogonal to all previous ones. In order to start the recursion, we choose either $|0\rangle = |u_0\rangle$ *or* $|0\rangle = |v_0\rangle$.

Having generated the sets of self-energies and off-diagonal coupling energies from the starter $|0\rangle = |u_0\rangle$, two diagonalizations (using TQLRAT) yield eigenvalues of **J**, denoted $\{E_\alpha\}$, and eigenvalues of the reduced Jacobi matrix in which (b_1 is set to zero), denoted $\{E_\alpha^{(u)}\}$. From these two sets of eigenvalues, all residues $R_u(\alpha)$ are computed from Eq. (20). Priming the recursion method with the other starting vector $|0\rangle = |v_o\rangle$ then leads to two additional sets of eigenvalues $\{E_\alpha\}$ and $\{E_\alpha^{(v)}\}$. (Of course, eigenvalues of the two full J matrices will be identical, for the $|u_0\rangle$ or $|v_0\rangle$ starting vectors.) The residues $R_v(\alpha)$ are then computed from an equation analogous to Eq. (20). The transition residues $R_{if}(\alpha)$ then follow very simply from Eq. (17).

A significant feature of the recursion method (mentioned earlier in connection with the optimal reduced space) is that the number of chain links n needed for convergence is usually *much smaller* than N, the size of the original molecular basis. As recursion proceeds, each chain link generates a more distant environment of the transition of interest. As a result, the eigenvalues and largest residues which are most important for the $i \to f$ transition are generated quickly; refinement of these values along with the generation of small residues and their eigenvalues occurs as n

increases. This feature has been demonstrated elsewhere [1, 2] for multiphoton excitation; a similar situation occurs in applications to solid state physics [10], and in the calculation of ESR lineshapes [21, 22].

As recursion proceeds, rounding errors in finite precision arithmetic lead to loss of significant figures which produces a gradual (after 30–50 steps) loss of global orthogonality (and linear independence) in the recursion basis. Numerical experience has shown that this results in multiple copies ("ghosts") of some eigenvalues, usually those on the edges of the range of eigenvalues. In addition, some "incorrect eigenvalues" (i.e., eigenvalues which are poor approximations to any real eigenvalues) are produced, which eventually settle onto actual eigenvalues as n increases. These *spurious eigenvalues* [8] must be removed from the eigenvalue lists before computing residues from Eq. (24). This is accomplished in a two-step procedure, as discussed elsewhere [1, 2]; it is an application of the Cullum–Willoughby method. The validity of the method for our application was established by comparing eigenvalues from direct diagonalization with those from the recursion procedure.

It is important to remove the multiple eigenvalues before using Eq. (22) to evaluate residues. Since different numbers of ghost eigenvalues may occur for each eigenvalue of both the full matrix $\mathbf{M}$ and the reduced matrix $\mathbf{M}^r$, it is essential to remove multiple copies from both lists $\{E_\alpha\}$ and $\{E_\alpha^{(u)}\}$. However, eigenvalues which appear in *both* lists (denoted "spurious" by Cullum and Willoughby) lead to cancelling contributions to Eq. (22), so they do not have to be removed from either list. A necessary, but not sufficient, check on the residues is the upper bound $R_u(\alpha) < 1$ and the sum rule $\sum_\alpha R_u(\alpha) = 1$. In practice, the sum rule is obeyed to within machine precision.

Computations with the Lanczos recursion procedure are greatly aided if $\mathbf{M}$ is a sparse matrix. For the algebraic Hamiltonian in Section II A, this is the case; the fraction of nonzero elements is generally less than 5%. Since there is discernable symmetry in the pattern of off-diagonal elements (e.g., repeating blocks of nonzero elements in each off-diagonal), our specialized multiplier (for obtaining $\mathbf{M}|u_j\rangle$) greatly speeds up the recursion process. This makes it possible to solve problems *in fast storage* that were far beyond the scope of any previous method (e.g., $N \sim 40{,}000$).

II. Results

In this section, time-dependent results will be shown for one case: a pump mode interacting with four bath modes ($n_\beta = 4$), with a maximum of 5 states per mode. This gives a total basis size of $N = 5^5 = 3125$. For the Hamiltonian parameters listed in Table 1, Band 1 ($E \sim 0$) has one state, Band 2 ($E \sim 1$) has five states, etc. In all of the cases considered here, V_{rad}, which controls the pump mode-laser interaction, will be held constant, while V_i, which determines the pump mode-bath mode interaction, will be increased in a series of steps from $\frac{1}{4}V_{\text{rad}}$ to $1\frac{1}{4}V_{\text{rad}}$. The ground

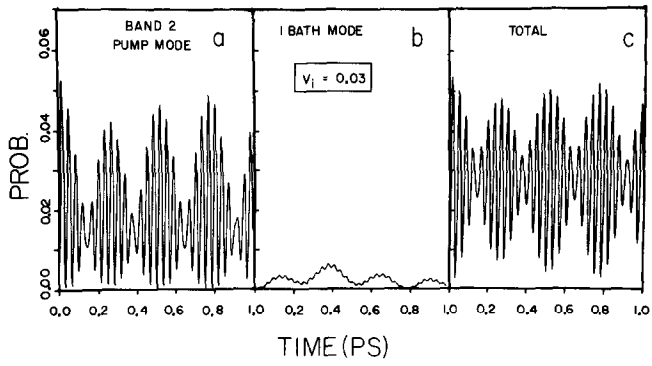

FIG. 2. Time-dependent transition probabilities for Band 2, $V_i = \frac{1}{4}V_{\text{rad}}$: (a) ground state-pump mode probability; (b) ground state-bath mode probability; (c) total transition probability to Band 2.

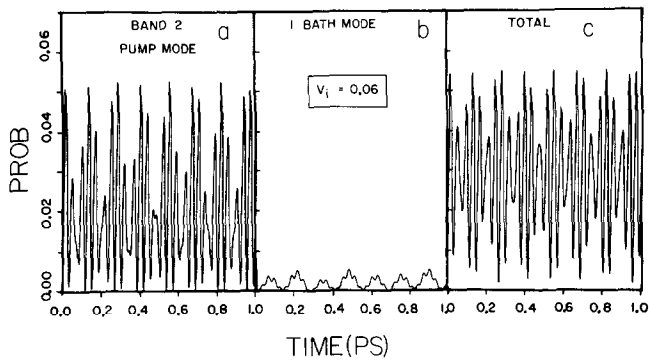

FIG. 3. Same as Fig. 2, except that $V_i = \frac{1}{2}V_{\text{rad}}$.

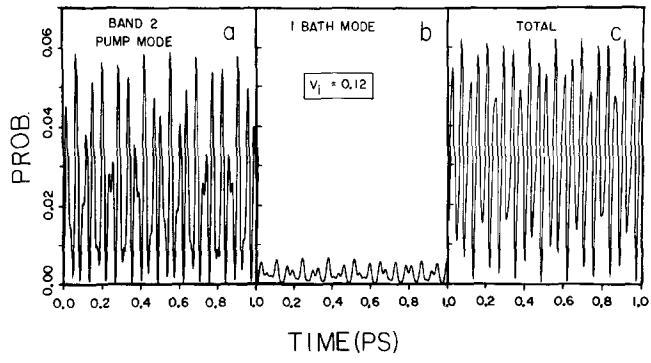

FIG. 4. Same as Fig. 2, except that $V_i = V_{\text{rad}}$.

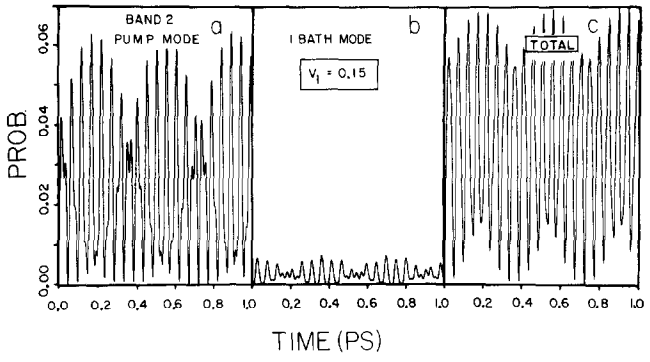

FIG. 5. Same as Fig. 2, except that $V_i = 1\frac{1}{4}V_{\text{rad}}$.

state-pump mode transition probability, the ground state-bath mode (for one bath mode in the band) transition probability, and the total transition probability (summed over the pump and bath modes) will be illustrated for Bands 2 (5 states) and 3 (15 states).

Figure 2 shows transition probabilities to Band 2, for weak intramolecular coupling, $V_i = \frac{1}{4}V_{\text{rad}}$. In part (a), there is a strong beating pattern in the pump mode transition probability due to interference between high frequency pump mode Rabi oscillations and the low frequency bath-pump mode interaction. Note that the pump mode probability rises quickly, before the bath modes have time to respond. In part (b), the probability in one bath mode is shown; probabilities for the other bath modes are qualitatively similar. The slow, reversible exchange of probability between the pump and bath modes is evident when parts (a) and (b) are compared. Finally, part (c) shows the total band probability. The envelope minima near $t = 0.15$, 0.40, 0.65, and 0.90 in part (a) have largely been filled in (due to bath mode excitations peaking at these times).

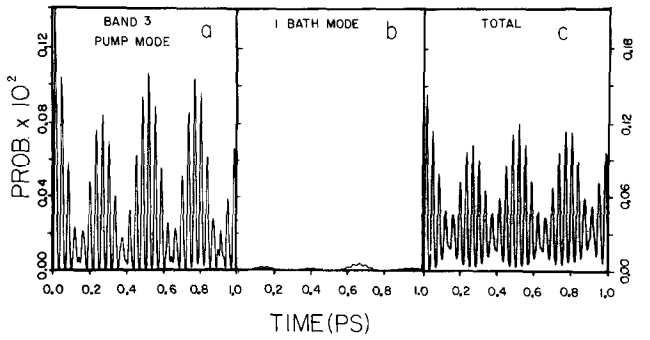

FIG. 6. Time-dependent transition probabilities for Band 3. The right ordinate applies to part (c) only.

TABLE II

Central Processor Times (CYBER 170/750) for Different Basis Sets[a]

N	CPU(sec)[b]
3,125	20
5,000	27
12,960	60
24,010	100
36,864	159

[a] In all cases, the I/O times were 7 sec.
[b] 100 recursion steps were used.

Figures 3–5 show similar results for Band 2, for increasing values of V_i, $V_i = \frac{1}{2}V_{\text{rad}}$, $V_i = V_{\text{rad}}$, and $V_i = 1\frac{1}{4}V_{\text{rad}}$. Increasing the frequency of the pump-bath probability interchange has a significant effect upon both the pump (part (a)) and the total probabilities (part (c)). First, in comparing Fig. 3a to Fig. 2a, note the more rapid fall off in the pump excitation at early times, due to the shorter response time of the bath. In Fig. 4, in contrast with Fig.s 2, 3, and 5, regular beating patterns in parts (a) and (c) have been replaced by a rather jagged sequence of maxima and minima. In Fig. 5, where $V_i > V_{\text{rad}}$, sudden growth of excitation in the bath modes robs probability from the pump mode. In Fig. 5(b), the effect of rapid pump-bath probability interchange is particularly evident at early times.

Figure 6 shows results for Band 3 (once again, $V_i = \frac{1}{4}V_{\text{rad}}$), which contains 15 states. In part (a), note that the maximum probability reaches only 0.0014, about 3% of the value in Band 2. In each part of this figure, the same high and low frequencies that appeared in Fig. 2 are again apparent. This is because all amplitude that enters band must come through Band 2, thus providing a good example of sequential, rather than direct, multiphoton absorption.

Central processor times for one transition, as a function of the basis size N, for a fixed number of recursion steps n, are listed in Table II. CPU times are approximately linear in both N and n.

IV. Conclusions

The recursive residue generation method was presented in the context of a time evolving molecule driven by a classical laser field. The molecular Hamiltonian was that of an anharmonic oscillator, linearly coupled to a harmonic bath with n_β degrees of freedom. The harmonic oscillator representation of the sparse Hamiltonian matrix was shown to have considerable structure, both in the locations of off-diagonal elements, and in the periodically repeating sets of values within each off-diagonal. Recognition of this structure allowed construction of a

smart matrix–vector multiplier. This multiplier, when incorporated in a minimal storage version of the Lanczos algortihm, allowed calculations on systems with much larger bases, and and at greatly reduced computation time per transition, than in our earlier studes [1, 2].

The time evolution of a system with 3125 states was studied in detail. Plots of state-to-state transition probabilities, for a range a laser–molecule coupling strengths, generally showed rapid excitation of the pump mode states, followed by reversible excitation of the bath states within the same band of quasidegenerate molecular states.

The RRGM, with utilization of structured sparsity, will allow a much more extensive computational study of a number of problems in quantum dynamics. Further apllications to laser driven molecules [37, 38], and to the evaluation of quantum mechanical time-dependent correlation functions [39] will be presented elsewhere.

ACKNOWLEDGMENTS

For helpful discussions, we thank David Scott, André Nauts, and Kent Milfeld.

REFERENCES

1. A. NAUTS AND R. E. WYATT, *Phys. Rev. Lett.* **51** (1983), 2238.
2. A. NAUTS AND R. E. WYATT, *Phys. Rev. A* **30** (1984), 872.
3. C. LANCZOS, *J. Res. Nat. Bur. Stand.* **45** (1950), 255.
4. B. N. PARLETT, "The symmetric Eigenvalue Problem," Chol. 13, Prentice–Hall, Englewood Cliffs, N. J., 1980.
5. C. MOLER AND I. SHAVITT (Eds.), "Numerical Algorithms in Chemistry: Algebraic Methods," NRCC, Lawrence Berkeley Labs., 1978.
6. C. C. PAIGE, *J. Inst. Math. Appl.* **10** (1972), 373; (1976), 341.
7. B. N. PARLETT AND D. S. SCOTT, *Math. Comp.* **33** (1979), 217.
8. J. CULLUM AND R. A. WILLOUGHBY, *J. Compute Phys.* **44** (1981), 329.
9. R. HAYDOCK, *Comp. Phys. Comm.* **20** (1980), 11.
10. R. HAYDOCK, *Solid State Phys.* **35** (1980), 215.
11. R. HAYDOCK, "Excitations in Disordered Systems" (R. Thorpe, Ed.), p. 29, (Plenum, New York, 1981.
12. S. MURAMATSU AND N. SAKAMATO, *J. Phys. Soc. Japan* **46** (1979), 1273.
13. N. SAKAMATO AND S. MURAMATSU, *Phys. Rev. B* **17** (1978), 868.
14. S. N. EVANGELOU, M. C. M. O'BRIEN, AND R. S. PERKINS, *J. Phys. C* **13** (1980), 4175.
15. M. C. M. O'BRIEN AND S. N. EVANGELOU, *J. Phys. C* **13** (1980), 611.
16. J. R. FLETCHER AND D. R. POOLER, *J. Phys. C* **15** (1982), 2695.
17. E. HALLER, H. KÖPPEL, L. S. CEDERBAUM, W. VON NIESSEN, AND G. BIERI, *J. Chem. Phys.* **78** (1983), 1359.
18. E. HALLER, H. KÖPPEL, AND L. S. CEDERBAUM, to be published.
19. A BARAM, *Mol. Phys.* **45**, (1982), 309.
20. S. ALEXANDER, A. BARAM, AND Z. LUZ, *J. Chem. Phys.* **61** (1974), 992.
21. G. MORO AND J. H. FREED, *J. Phys. Chem.* **84** (1980), 2837.
22. G. MORO AND J. H. FREED, *J. Chem. Phys.* **74**, (1981), 3757.

23. P. W. LANGHOFF, "Methods in Computational Molecular Physics" (G. H. Diercksen and S. Wilson, Eds.), p. 299, Reidel, Dordrecht, 1983.
24. M. R. HERMANN AND P. W. LANGHOFF, *Int. J. Quantum Chem.* **23** (1983), 135.
25. J. R. ACKERHALT, H. W. GALBRAITH, AND P. W. MILONNI, *Phys. Rev. Lett.* **51** (1983), 1259.
26. M. S. SLUTSKY AND T. F. GEORGE, *Chem. Phys. Lett.* **57** (1978), 474.
27. E. MERZBACHER, "Quantum Mechanics," p. 62, Wiley, New York, 1962.
28. R. A. FRIESNER, Private communication.
29. M. L. GOLDBERGER AND K. M. WATSON, "Collision Theory," Chap. 8, Wiley, New York, 1964.
30. L. MOWER, *Phys. Rev.* **142** (1966), 799.
31. P. PECHUKAS AND J. C. LIGHT, *J. Chem. Phys.* **44** (1965), 3897.
32. D. W. ROBINSON, *Helv. Phys. Acta* **36** (1963), 140.
33. K. F. MILFELD AND R. E. WYATT, *Phys. Rev. A* **27** (1983), 72.
34. S. R. BARONE, M. A. NARCOWICH, AND F. J. NARCOWICH, *Phys. Rev. A* **15** (1977), 1109.
35. F. GESZTESY AND H. MITTER, *J. Phys. A* **14** (1981), L79.
36. R. P. TEWARSON, "Sparse Matrices," Chap. 1, Academic Press, New York, 1973.
37. K. F. MILFELD, JOSÉ E. CASTILLO, AND R. E. WYATT, to be published.
38. J. CHANG, S. L. DING, AND R. E. WYATT, to be published.
39. R. A. FRIESNER AND R. E. WYATT, *J. Chem. Phys.* **82** (1985), 1973.